Multifunctional Up-Converting Nanocomposites with Smart Polymer Brushes Gated Mesopores for Cell Imaging and Thermo/pH Dual-Responsive Drug Controlled Release

Xiao Zhang, Piaoping Yang, Yunlu Dai, Ping'an Ma, Xuejiao Li, Ziyong Cheng, Zhiyao Hou, Xiaojiao Kang, Chunxia Li, and Jun Lin**

Multifunctional nanocarriers based on the up-conversion luminescent nanoparticles of $NaYF_4$:Yb^{3+}/Er^{3+} core (UCNPs) and thermo/pH-coupling sensitive polymer poly[(*N*-isopropylacrylamide)-*co*-(methacrylic acid)] (P(NIPAm-*co*-MAA)) gated mesoporous silica shell are reported for cancer theranostics, including fluorescence imaging, and for controlled drug release for therapy. The as-synthesized hybrid nanospheres UCNPs@mSiO_2-P(NIPAm-*co*-MAA) show bright green up-conversion fluorescence under 980 nm laser excitation and the thermo/pH-sensitive polymer is active as a "valve" to moderate the diffusion of the embedded drugs in-and-out of the pore channels of the silica container. The anticancer drug doxorubicin hydrochloride (DOX) can be absorbed into UCNPs@mSiO_2-P(NIPAm-*co*-MAA) nanospheres and the composite drug delivery system (DDS) shows a low level of leakage at low temperature/high pH values but significantly enhanced release at higher temperature/lower pH values, exhibiting an apparent thermo/pH controlled "on-off" drug release pattern. The as-prepared UCNPs@mSiO_2-P(NIPAm-*co*-MAA) hybrid nanospheres can be used as bioimaging agents and biomonitors to track the extent of drug release. The reported multifunctional nanocarriers represent a novel and versatile class of platform for simultaneous imaging and stimuli-responsive controlled drug delivery.

1. Introduction

Recent advances in nanomedicine have heightened the demand for new therapies and coherent implementation of next generation of nanoplatforms for the integration of medical diagnostics, drug delivery and efficient therapy (theranostics) into a single structured nanodelivery system.[1] Benefiting from the significantly improved physical, chemical, and biological properties, multifunctional nano-materials offer an opportunity for bioimaging and simultaneous diagnosis and therapy.[2] Fluorescence is now becoming one of the key detection methods in genomics, proteomics and cell biology. Along these lines, the attractive platform based on luminescent nanoparticles have been used as biolabeling, leading recently major advances in biological and biomedical imaging.[3] The biological luminescent materials, upconversion nanoparticles (UCNPs), show attractive merits including narrow emission peak, nonblinking emission,[4] long lifetimes, excellent photostability[5] and low toxicity.[6] More importantly, UCNPs are excited by NIR light, which is located in the "optical transmission window" of the biological tissues in which blood and tissue are maximally transparent.[7] Such unique advantages make upconversion luminescence (UCL) imaging to be a favorable visualizing tool with slight photodamage, low autofluorescence background, high detection sensitivity, and greater tissue penetration depth in biological tissues.[3,i,7,8] For example, Wang and co-workers load Chloring e6, a photosensitizer, on polymer-coated UCNPs, forming a UCNP-Ce6 supramolecular complex. Such hybrid materials can produce singlet oxygen to kill cancers under NIR light. Compared to the traditional PDT relying on visible light excitation, the NIR light shows its advantage for a much deeper tissue penetration depth and obtained a better in vivo tumor growth inhibition efficacy.[7] Yb, Er co-doped β-$NaYF_4$ has been proved to be one of the most efficient NIR-to-vis upconversion fluorescnet materials for performing multicolor UC emission, and has been employed in cells, tissues and in vivo animal imaging.[3,f,,7,9] In particular, the construction of multifunctional nanocomposites composed of mesoporous silica and UCNPs have been a research hotspot in the forefront of materials science.[1,a,,5,10] Mesoporous silica nanoparticles (MSNs) have been recently employed as robust inorganic scaffolds for the storage and release of drugs thanks to its unique

Dr. X. Zhang, Dr. Y. Dai, Dr. P. Ma, Dr. X. Li,
Dr. Z. Cheng, Dr. Z. Hou, Dr. X. Kang,
Dr. C. Li, Prof. J. Lin
State Key Laboratory of Rare Earth Resource Utilization
Changchun Institute of Applied Chemistry
Chinese Academy of Sciences
Changchun 130022, P. R. China
E-mail: zycheng@ciac.jl.cn; jlin@ciac.jl.cn
Dr. X. Zhang, Prof. P. Yang
Key Laboratory of Superlight Materials and surface Technology
Ministry of Education
College of Materials Science and Chemical Engineering
Harbin Engineering University
Harbin 150001, P. R. China

DOI: 10.1002/adfm.201300136

features, such as remarkable biocompatibility, stability, and large loading capacity. More importantly, the abundant silanol groups (Si-OH) that tile their pore channels and surfaces facilitate the possibility to include gate-like scaffoldings on the external/internal surface, thereby simplifying the design of nanodevices for on-command delivery applications.[11] Integration of mesoporous silica with upconversion monodisperse nanocrystals to form uniform core–shell composite particles will endow the nanocomposite functions of bioimaging and drug delivery with good biocompatibility and chemical stability simultaneously.

Since traditional anticancer drugs cannot distinguish between cancerous and healthy cells, collateral damage and adverse side effects are almost inevitable. To address this formidable challenge, mesoporous silica based nanocontainers equipped with "gatekeepers" are enormously appealing as delivery vehicles, in which a regulated release of cargos at specific time interval and required site can be achieved by taking advantage of various "gatekeepers".[12] To date, different kinds of pore blocking caps, such as nanoparticles,[13] organic molecules,[14] and polymer chains or brushes[15] have been introduced onto the surface or pore channels to keep compounds from leaching out and to permit their controlled release. Poly(*N*-isopropylacrylamide) (PNIPAm), the most prominent temperature-sensitive polymer, exhibits a reversible phase transition in aqueous solution, thus is suitable for blocking pores to program the drug release.[16] In addition, by incorporating comonomer units, such as MAA, the low critical solution temperature (LCST) of the PNIPAm homopolymer can be tuned to be above normal body temperature (37 °C). Currently, typical biological stimuli, is exploited for favored drug release including pH and temperature. Most solid tumors have a weakly acidic extracellular environment (pH = 6.0–7.0) than normal tissues and bloodstream (pH = 7.4) due to the hypoxia-induced coordinated upregulation of glycolysis, and pH still drops further inside cells, especially, inside endosomes (pH = 5–6) and lysosome (pH = 4–5).[17] Additionally, the local characteristic for certain malignancies show distinct hyperthermia.[18] More importantly, the faster drug release at increased temperature, noted as positive temperature controlled "on-off" drug release, in some cases, is more attractive because it can respond to an increased body temperature arising from diseases such as inflammation or cancers.[19] Consequently, theses features could be used for feasibly designing multisensitive carriers that intelligently distinguish between normal and tumor tissues, achieving better targeting efficiency and treatment efficacy.

However, previous work mainly focused on fabrication of magnetic silica nanoparticles together with smart polymers for diagnosis and treatment.[16,b,16d,20] Moreover, the conventional process to produce the uniform core-shell materials consisting of oleic acid capped UCNPs and mesoporous silica usually requires the intermediate coatings of solid silica and calcination process, which lead to the complicated procedure and difficulties for post functionalization. Our group has previously combined the lanthanide doped up-conversion luminescent materials with stimuli-responsive polymer network for drug release.[21] However, PNIPAm used as drug carriers suffered from a poor stability when they are exposed under physiological environment owing to biochemical attack such as protein adsorption or changed ionic-strength effect, which may disturb the responsive properties of PNIPAm. Additionally, it is still a challenge for preventing the leakage and degradation of the drug encapsulated in a polymer network. Moreover, the surface attached polymer brushes can response faster for the external stimuli compared with cross-linked polymer network because the movement of the macromolecular segments are less constrained. Up to now, few reports are presented on the fabrication of lanthanide doped up-conversion luminescent materials decorated by polymers blocked mesopores nanocontainer for stimuli-responsive drug release and bioimaging.

In this study, we assess the potential of this device to combine luminescent image and anticancer thermotherapy with triggered drug release under controlled stimulus, wherein UCNPs were directly encapsulated in uniform mesoporous silica shell, and then poly(*N*-isopropylacrylamide-*co*-methacrylic acid) [P(NIPAm-*co*-MAA)] polymer brushes were grafted onto the channel and outer shell of the mesoporous silica scafford. The design of the architecture was expected to block off the pores at low temperature/high pH and reopen at high temperature/low pH values reversibly. The obtained hybrid nanocarriers were capable of loading anti-cancer drug doxorubicin (DOX) and respond to the slight difference of temperature/pH between tumor tissue and healthy tissue in the simulated physiological conditions. In addition, the shrink of the polymer brushes induced by photothermal effects of NIR irradation also promoted the release of DOX molecules from the composites. Moreover, the composite nanospheres were highly biocompatible in vitro and amenable to upconversion luminescence imaging, endowing the nanocomposite bifunctional properties under NIR irradiation. In fact, the thermal/pH dependent drug release combined with NIR laser remote triggering provides the possibility of flexible control of location, dose magnitude and timing.

2. Results and Discussion

β-$NaYF_4$: Yb^{3+}/Er^{3+} nanoparticles (UCNPs) were utilized as optical nanoprobe and the mesoporous silica shell acted both as drug carriers and nanoreactor. The linear P(NIPAm-*co*-MAA) brushes were introduced onto the channels and surfaces of the silica, which are thermo/pH-responsive, acting as the "gatekeepers" for the drug delivery vehicles. The synthetic process of UCNPs@mSiO_2-P(NIPAm-*co*-MAA) hybrid nanospheres and the mechanism of control delivery of drugs are summarized schematically in **Scheme 1**. Firstly, the UCNP cores, which were stabilized with hydrophobic oleic acid (OA) ligands and dispersed in nonpolar organic solvents, was synthesized through a facile thermal decomposition method. Then the hydrophobic UCNPs were transferred into an aqueous media by using cetyltrimethylammonium bromide (CTAB) as the capping molecules. Subsequently, the particles were encapsulated by a mesoporous silica shell via the hydrolysis of tetraethylorthosilicate (TEOS) in a microemulsion system. It is worth noting that CTAB could be used not only as the stabilizing surfactant for transferring hydrophobic UCNPs to the aqueous phase but also the organic templates for the formation of the mesoporous silica shells.[2,d,2k,,22] After removing CTAB, the

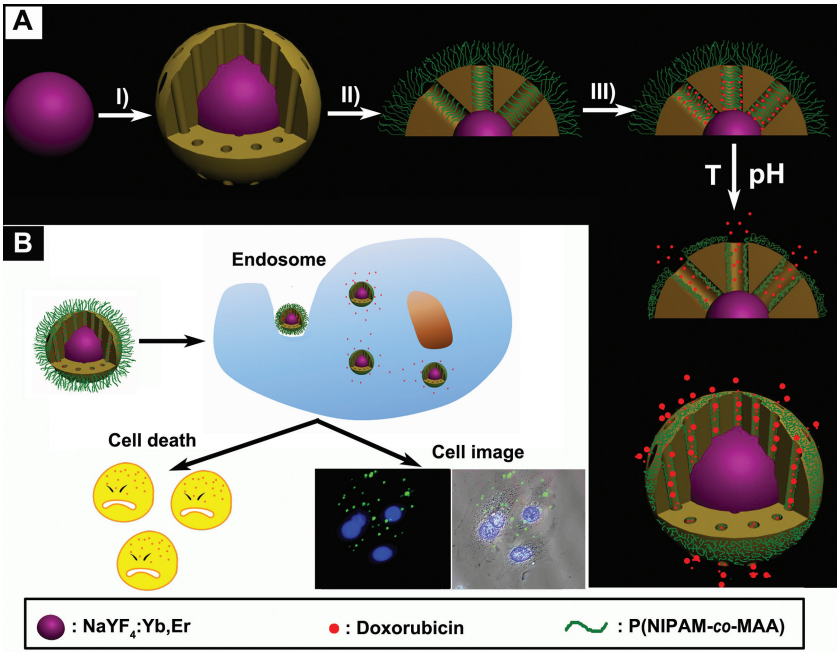

Scheme 1. A) Synthetic route to UCNPs@mSiO$_2$-P(NIPAm-*co*-MAA): I) cetyltrimethylammonium bromide, tetraethyl orthosilicate; II) methacryloxypropyltrimethoxysilane, *N*-isopropylacrylamide, methacrylic acid; III) guest (DOX) loading; IV) increase the temperature and decrease the pH value. B) Schematic depiction of the dual function of UCNPs@mSiO$_2$-P(NIPAm-*co*-MAA).

templating agent, methacryloxypropyltrim-ethoxysilane (MPS), was introduced onto the channel and the surface of the mesorpores silica, resulting in carbon-carbon double bonds which can graft a polymer chain in the process of polymerization. In an aim to achieve the smart stimuli-response drug delivery system, NIPAm and MAA monomers were copolymerized by photo-induced polymerization using MPS-modified mesoporous silica UCNPs as seeds, which resulted in the formation of the P(NIPAm-*co*-MAA) brushes blocked UCNPs@mSiO$_2$ hybrid nanospheres, denoted as UCNPs@mSiO$_2$-P(NIPAm-*co*-MAA) (Scheme 1A). The well-designed hybrid core/shell nanospheres can be used in bioimaging and be engineered to release drugs respond to the slight difference of temperature/pH between tumor tissue and healthy tissue in the simulated physiological conditions (Scheme 1B).

2.1. Preparation of UCNPs@mSiO$_2$-P(NIPAm-*co*-MAA) and Their Characterization

The initial oleic acid capped UCNPs (OA-UCNPs) core can only be dispersed in nonpolar solvents such as cyclohexane, chloroform and dichloromethane. As depicted in **Figure 1**, the as-prepared OA-UCNPs are uniform, and well dispersed in a solution of chloroform. The average diameter is about 24 nm according to the transmission electron microscopy (TEM) image (Figure 1A). The high-resolution TEM (HRTEM) image of UCNPs confirmed the high crystallinity of the particles with a d-spacing value of 0.52 nm, which is close to the d_{110} value of hexagonal-phase $NaYF_4$ (Figure 1B). These uniform cores resulted in a narrow distribution of the final particle sizes. After being coated with a thin mesoporous silica layer, UCNPs@mSiO$_2$ nanospheres still retain the morphological features of pure $NaYF_4$:Yb^{3+}/Er^{3+}. Figure 1C, D shows the TEM images of the SiO$_2$-coated UCNPs, which display a narrow size distribution. Each UCNP, the central dark spot as a core in the middle, was evenly encapsulated by a 9 nm thick silica layer and the worm-like channel can be clearly observed. The inner channel and the out surface of the mesoporous silica were utilized as scaffold for successfully grafting smart P(NIPAm-*co*-AAm) polymer brushes via photo-induced polymerization to form the multifunctional composite nanosphere. As shown in Figure 1E, F, the rough surfaces were clearly observed and a bright ring around the composite particles was presented due to the different electron penetrability for the cores and polymer shells.

Figure S1 (Supporting Information) reveals the XRD patterns of as-synthesized UCNPs, UCNPs@mSiO$_2$ and UCNPs@mSiO$_2$-P(NIPAm-*co*-MAA) composites, as well as the standard data for β-$NaYF_4$ (JCPDS:16-0334) respectively. As for the obtained oleic acid stabilized UCNPs, all the diffraction peaks can be readily indexed to pure hexagonal $NaYF_4$ (JCPDS: 16-0334) shown in Figure S1A (Supporting Information). XRD pattern of the as-obtained UCNPs@mSiO$_2$ nanocomposites (Figure S1B, Supporting Information) shows a broad diffraction peak of amorphous silica at $2\theta = 22°$ besides the characteristic sharp peaks of UCNPs, indicating the successful coating of silica shell. After polymerizing the NIPAm and MAA monomer on the silica scaffold, the XRD pattern (Figure S1C, Supporting Information) does not change much.

Fourier transform infrared (FTIR) spectra also provided clear evidence for the formation procedure of the multifunctional nanocomposites (**Figure 2**). As shown in Figure 2A, the FTIR spectrum of oleic-acid-coated UCNPs showed characteristic bands of oleyl chains. The 2925 and 2854 cm^{-1} peaks are assigned to the asymmetric (ν_{as}) and symmetric (ν_s) stretching vibration of methylene (CH_2) in the long alkyl chain of the oleic acid molecule, respectively. The 1566 and 1467 cm^{-1} transmission bands can be ascribed to the asymmetric (ν_{as}) and symmetric (ν_s) stretching vibration of the carboxylic carboxylic group (–COOH), respectively. Concomitant with the encapsulation by the mesoporous silica shell, the obvious peaks at 1083 and 802 cm^{-1} are attributed to the vibration bands of Si-O-Si, whereas the peaks at 947, 1630, and 3432 cm^{-1} belong to Si-OH, H_2O, and -OH, suggesting that a large number of OH group and H_2O molecules exist on the surfaces of the particles (Figure 2B), which play a key role for adsorbing drug molecules by hydrogen bond. In the case of the MPS-modified core-shell composite, showing C=O stretching at 1720 cm^{-1} and -CH_2 stretching at 2958 cm^{-1} (Figure 2C), indicating the successful functionalization.[23] In the spectrum of UCNPs@mSiO$_2$-P(NIPAm-*co*-

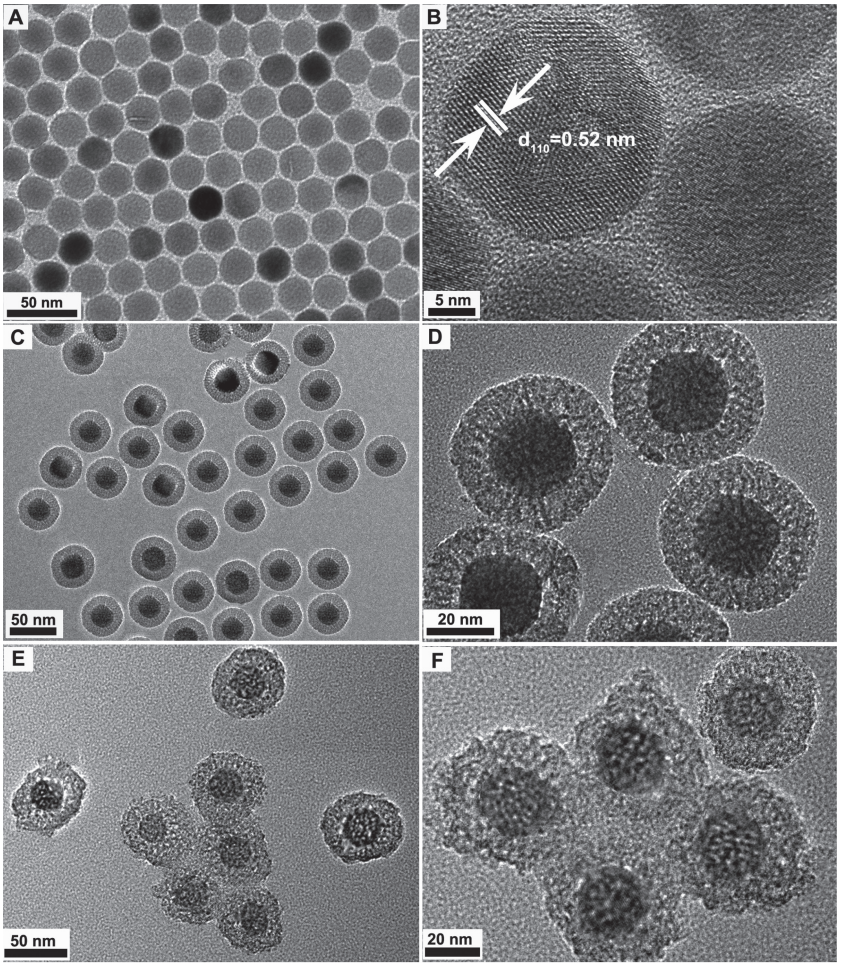

Figure 1. A) TEM and B) HRTEM images of $NaYF_4$:Yb^{3+}/Er^{3+} (18/2 mol%) nanoparticles (UCNPs). C) Low- and D) high-magnificationTEM images of UCNPs@$mSiO_2$. E) Low- and F) high-magnification TEM images of UCNPs@$mSiO_2$-P(NIPAm-co-MAA).

MAA) (Figure 2D), the appearance of characteristic IR peaks at 1643 and 1550 cm^{-1} should be attributed to the secondary amide C=O stretching and N-H bending vibrations, respectively. In addition, the band at 1458 cm^{-1} is corresponding to the bending vibration of C-H while the bands at 1388 cm^{-1} is attributed to the deformation of methyl groups on–$C(CH_3)_2$ belonged to the characteristic peaks of PNIPAm. These results confirmed the successful copolymerization of NIPAm and MAA onto the UCNPs@$mSiO_2$ nanoreactor. Such process can also be confirmed by tracking the surface property of the materials through zeta-potential measurement. Notably, template CTAB is hazardous and less biocompatible, which should be removed before any bioapplications.[2,d,24] Before washing, a negatively charged surface of –11.1 mV is presented. The gradual removal of the CTAB surfactant after ion exchange procedures is reflected from the decrease of the zeta-potential measurements, stabilizing to a negatively charged –16.7 mV. To further demonstrate the successful MPS modification and P(NIPAm-*co*-MAA) polymerization, the results of zeta-potential measurement were also exhibited. MPS modified showed the similar change trend with a negatively charged –8.2 mV. However, the presence of P(NIPAm-*co*-MAA) drastically changed the surface property and offered a more negatively charged surface of –23.4 mV. This observation provided good evidence that CTAB has been removed and the successfully polyermerision of P(NIPAm-*co*-MAA) onto the UCNPs@$mSiO_2$ seeds.

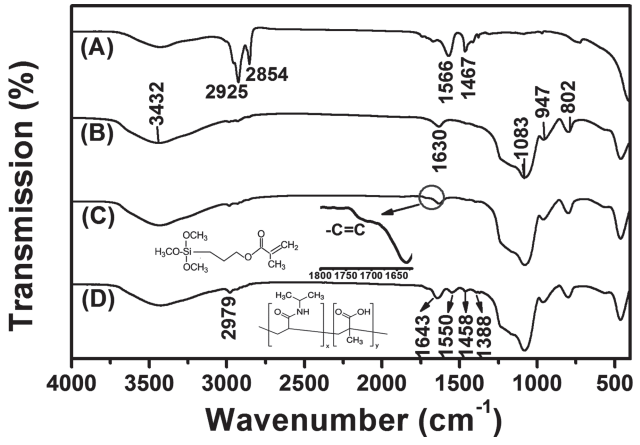

Figure2. FTIR spectra of A) oleic acid stablized UCNPs, B) UCNPs@$mSiO_2$, C) UCNPs@$mSiO_2$-MPS and D) UCNPs@$mSiO_2$- P(NIPAm-*co*-MAA).

The polymer brushes introduced onto the surfaces and channels of the mesorpors were expected to be used as gatekeepers for drug controlled release. The molecular weight and polydispersity of the polymers was confirmed by using gel permeation chromatography (GPC) measurements. We suppose the polydispersity of the polymer brushes attached onto the mesoporous silica is similar with its supernate. The molecular weights of P(NIPAm-*co*-MAA) existing in supernate is measured to be M_w = 75417 g/mol and it had a unimodal molecular weight distribution of M_w/M_n = 1.58. To determine the quantitative amount of the organic content loaded into the UCNPs@$mSiO_2$ nanoreactor, thermogravimetry (TG) was employed to directly measure the weight loss of as-prepared product, as shown in Figure S2 (Supporting Information). Compared with particles synthesized without P(NIPAm-*co*-MAA), the organic-inorganic composites of UCNPs@$mSiO_2$-P(NIPAm-co-MAA), however, a relatively high decrease of 16.5% in weight is found, indicating that the polymer content is about 16.5 wt% in the composites. Also as detailed in Figure S3 (Supporting Information), the isotherms of the two samples can be classified as type IV with typical H1 hysteresis loop, which demonstrate the presence of textual mesoporous. The BET surface area, total pore volume and Barret-Joner-Halenda (BJH) pore diameters of UCNPs@$mSiO_2$ nanocomposite were estimated to be 770 m^2/g, 0.95 cm^3/g, and 2.74 nm, respectively. After polymerazation,

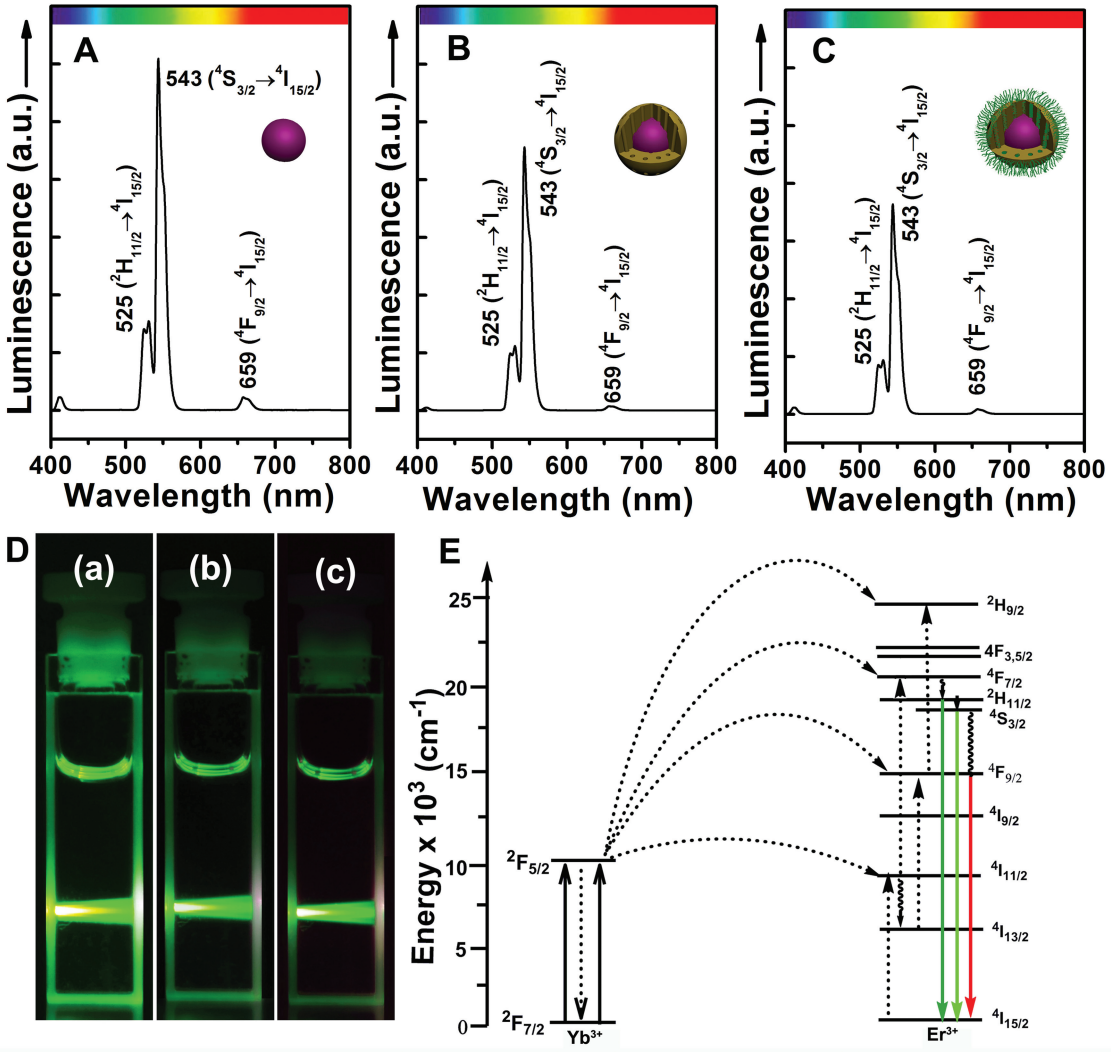

Figure 3. The emission spectra of the A) UCNPs; B) UCNPs@mSiO$_2$, and C) UCNPs@mSiO$_2$-P(NIPAm-*co*-MAA) nanoparticles under 980 nm laser diode excitation. D) Photographs of corresponding luminescent nanoparticles of the colloidal solutions dispersed in DMSO under a 980 nm lamp. The particle concentration for all samples was 5 mg/mL in DMSO. E) Schematic energy-level diagrams of the Yb^{3+}, Er^{3+} ions and the UC mechanism excited by 980 nm laser diode. The solid, dotted, and curly arrows indicate radiative, non-radiative energy transfer, and multiphoton relaxation processes, respectively.

the Brunauer-Emmett-Teller (BET) surface area of UCNPs@mSiO$_2$-P(NIPAm-*co*-MAA) is about 368 m^2/g, pore volume is about 0.67 cm^3/g and BJH pores diameters exhibit dual mode with 2.19 and 1.41 nm. The sharply degreasing along with the grafting processes could be interpreted as mesopores of UCNPs@mSiO$_2$ being sealed by P(NIPAm-*co*-MAA) polymer.

Lanthanide-doped upconversion nanoparticles usually offer high photostability and enable deep tissue-penetration depths (up to 10 mm) by irradiation with near-infrared (NIR) light, which makes them particularly attractive for bioimaging applications.[8b,9a-9b,21] In our present work, obviously, all solutions of unmodified, silica-coated composite spheres and ploymer caped hybrid nano-materials have similar emissions except for the decrease of intensity in the visible spectral regions under irradiation with NIR light (**Figure 3**A–C), which demonstrates that coating the UCNPs with a silica and polymer shell did not significantly affect the upconversion properties. All spectra of the three samples have a primary strong band in the green emission region maximized at 543 nm assigned to the $^4S_{3/2} \rightarrow {}^4I_{15/2}$ of Er^{3+}, and the weak band in the red region at 659 nm due to the $^4F_{9/2} \rightarrow {}^4I_{15/2}$ transition of Er^{3+}.[25] The much stronger green emission than the red light results in the bright green emission. More intuitively, the corresponding luminescent photos of the colloidal solutions in DMSO all show green output with a gradually decreasing trend (Figure 3Da,b,c). The proposed UC energy transfer mechanisms were well investigated and depicted in Figure 3E. As the initial energy transfer, under the 980 nm NIR light, an electron of the Yb^{3+} ion is excited from the $^2F_{7/2}$ to $^2F_{5/2}$ level by the NIR light due to strong absorption at 980 nm of the Yb^{3+} ion, and then an excited Yb^{3+} transfer its energy to Er^{3+} ($^4I_{11/2}$). During the population of the $^4I_{11/2}$ level, a second 980 nm photon transferred by the excited Yb^{3+} ion can then populate a higher $^4F_{7/2}$ energetic state of the Er^{3+} ion, whose energy lies in the visible region. The Er^{3+} ion can then relax nonradiatively by a fast multi-phonon relaxation

process to the $^2H_{11/2}$ and $^4S_{3/2}$ levels and radiant transitions from these levels yield emissions at 525 nm ($^2H_{11/2}\rightarrow{}^4I_{15/2}$), 543 nm ($^4S_{3/2}\rightarrow{}^4I_{15/2}$), respectively. Alternatively, the electron can further relax and populate the $^4F_{9/2}$ level resulting in the occurrence of red $^4F_{9/2}\rightarrow{}^4I_{15/2}$ (659 nm) emission.[22,a,25,26]

For bioapplications, it is a crucial prerequisite to ensure the stability of the nanocarrier materials under physiological environment. Thus we also investigated the stability behavior of the UCNPs@mSiO$_2$-P(NIPAm-*co*-MAA) hybrid nanocarrier under different conditions. After silica-P(NIPAm-*co*-MAA) coating, the nanocarriers exhibit better water-solubility and were well dispersible in water. The chemical and photo-chemical stability of the hybrid UCNPs@mSiO$_2$-P(NIPAm-*co*-MAA) nanoparticles were well studied. As represented above, the prepared hybrid nanoparticles possess two emission bands in the green emission region maximized at 543 nm and the weak band in the red region at 659 nm under irradiation with 980 nm light. The composites were incubated in water or PBS for half a month and the fluorescence intensity of the nanoparticles was almost unchanged (Figure S4A,B, Supporting Information). Furthermore, no obvious change in fluorescence intensity was observed when the nanoparticles were incubated in water with different pH values (Figure S4C, Supporting Information). Obviously, the almost constant emission indicates that the samples are of high chemical stability. The hybrid nanoparticles were also continuously exposed to NIR laser and the intensity of the studied samples monotonously decreases with prolonging the irradiation time up to 7 h at a power of 1.22 W (Figure S4D, Supporting Information), and the results showed that the nanoparticles are photochemically stable.

2.2. In Vitro Cytotoxicity of The UCNPs@mSiO$_2$-P(NIPAm-*co* -MAA) Nanoparticles

The investigation of the cytotoxicity of the hybrid nanocarrier is crucial for its potential biomedical applications. Only nontoxic carriers are suitable for drug delivery. Here the cellular toxicity of UCNPs@mSiO$_2$-P(NIPAm-*co*-AAm) nanoparticles toward L929 fibroblast cells was determined by means of a standard MTT cell assay. It could be seen that P(NIPAm-*co*-AAm) coated UCNPs@mSiO$_2$ nanocomposites showed no significant cytotoxic effect on the L929 cells in a wide range of concentration (3.125-200 μg mL^{-1}). As depicted in Figure S5A (Supporting Information), the cell viability was attained 91.87% even the concentration of the UCNPs@mSiO$_2$-P(NIPAm-*co*-MAA) carriers as high as 200 μg mL^{-1} (the total content of the particles). Figure S5B,C (Supporting Information) show the inverted microscopy images of the cells grown in the presence of the hybrid nanospheres, which reveal that all cells spread and began to proliferate, and their density increased gradually. The above experimental results indicate that the nanocomposite samples have good biocompatibility and are potential to be used as drug carrier in biomedical application.

2.3. Drug Loading and Release Properties

We further investigated the controlled release of the UCNPs@mSiO$_2$-P(NIPAm-*co*-MAA) hybrid nanospheres. Doxorubicin hydrochloride (DOX), a commonly used chemotherapeutic drug for cancer therapy, was selected as a model drug to evaluate the loading and controlled release behaviors of the composite nanospheres. The actual loading level of DOX in the nanospheres is calculated to be 8.6% DOX in weight, as determined by the characteristic DOX optical absorbance at 480 nm. The in vitro release profiles of DOX from the DOX-loaded UCNPs@mSiO$_2$-P(NIPAm-*co*-MAA) nanospheres in PBS buffer in response to a temperature change between 20 and 45 °C is shown in **Figure 4**A–C, respectively. As can be seen in Figure 4A, besides an initial small burst effect due to the presence of the drug at the surface, the drug release reached a plateau at 9.6% DOX within 4 h and then remained little changed over hours due to the blocking effect of the loose polymer brushes. In contrast, the fast release of DOX at 45 °C was consistent with shrink of the P(NIPAm-*co*-MAA) brushes at high temperature. The system showed a rapidly released behavior and the cumulative release amount of DOX 39.5% within 24 h at physiological pH (7.4) at the high temperature (45 °C). Similar release trends were achieved when DOX-loaded UCNPs@mSiO$_2$-P(NIPAm-*co*-MAA) nanospheres immerse in PBS buffer solutions of lower pH values (pH = 4.5, 2.0), in which all possess a faster drug release profile at higher temperature (Figure 4B,C). Therefore, a temperature-responsive control release system has been successfully prepared. The temperature-sensitive polymer brushes play a significant role of controlled switch for drug release. We suppose that the polymer brushes stretches in a great extent in the cool medium (25 °C), however, the long polymer chain in the channel of the silica act as bolt to block the drug release to a certain extent. On the other hand, as the temperature was increased above the LCST of P(NIPAm-*co*-MAA), the polymer chain was forced to shrink to open the porous channels and enable the entrapped drug molecules to leak out. The temperature-sensitive polymer chains act as gatekeepers to control the drug release. In order to further vetify the blocking effect of polymer brushes, the release profile of DOX-loaded UCNPs@mSiO$_2$ and UCNPs@mSiO$_2$-P(NIPAm-*co*-MAA) were also carried out in Figure S6 (Supporting Information). The system without polymer gated nanocarrier showed a more rapidly released behavior at physiological pH (7.4) at the low temperature (25 °C) which indicate the loosed polymer brushes play an positive role in maintaining the drugs inside at lower temperature. Meanwhile, the crosswise comparison of Figure 4A–C indicates that pH values have significant effect for the confined DOX releasing from the mesopores. The drug release rate of DOX-loaded UCNPs@mSiO$_2$-P(NIPAm-*co*-MAA) composite was obviously speeded-up with the decrease of pH. By fixing the temperature at 25 °C for comparison, only 13% of DOX was released from the composite nanospheres even after 24 h at pH 7.4. With an increase of acidity to a mildly acidic conditions (pH 5.0) (Figure 4B), the DOX release rate reached to 52.2% after 20 h and more than 79.3% of DOX was released within 12 h in PBS of pH 2.0. This feature can be attributed to the small part of pH-sensitive PMAA component which induce the change of electrostatic forces between PMAA and drugs. At pH 7.4, the electrostatic attraction makes DOX difficult to release from carriers. At more acidic environment (pH 5.0 and pH 2.0), DOX can be released from carrier by diffusion-controlled mechanism due

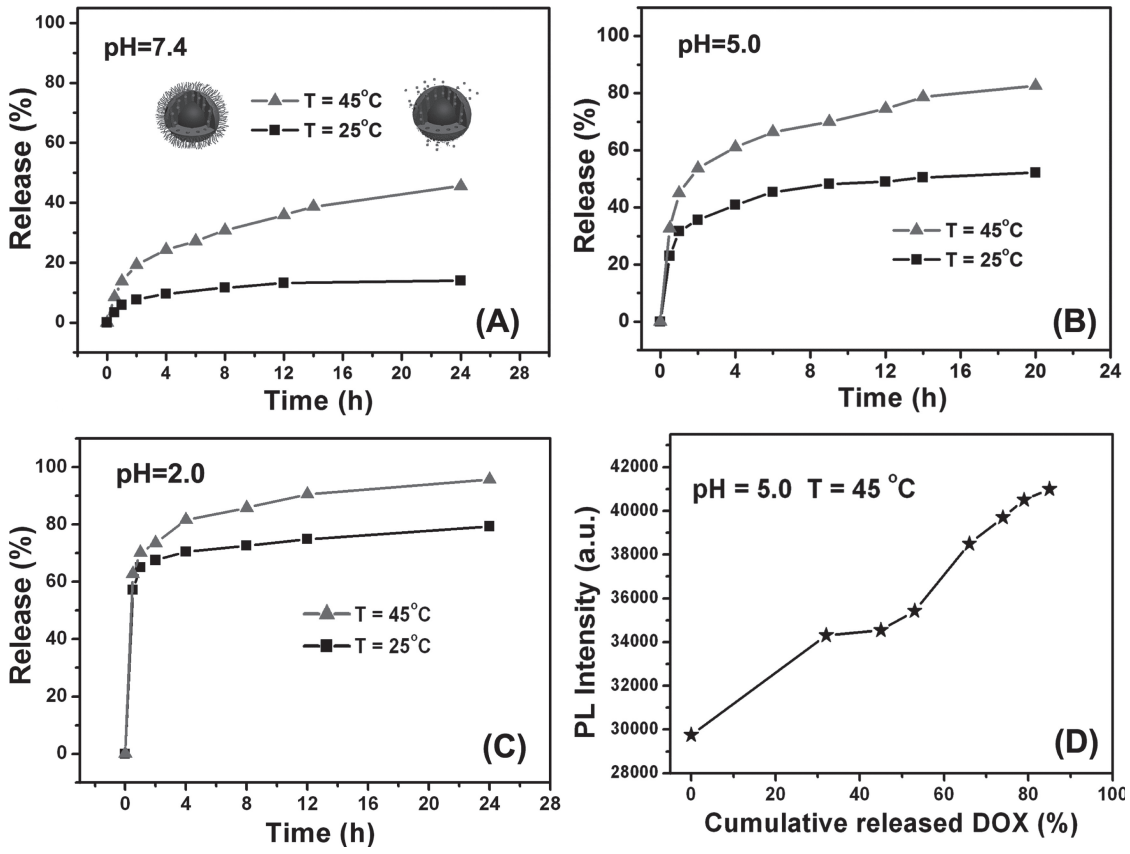

Figure 4. Release profiles of DOX-UCNPs@mSiO$_2$-P(NIPAm-co-MAA) in response to temperature changes in PBS: A) pH = 7.4; B) pH = 5.0 and C) pH = 2.0 The release of drug molecules was monitored using a UV-vis spectrophotometer. D) Upconversion emission intensity of UCNPs@mSiO$_2$-P(NIPAm-*co*-MAA) as a function of the cumulatively released DOX.

to the reduced electrostatic forces between PMAA and drugs. Meanwhile, the results can also be explained to be pH-induced thermally responsive drug release property as reported previously.[21] The critical solution temperature (LCST) of the P(NIPAm-*co*-MAA) brushes become lower as decreasing the pH value when fixing a temperature. As a result, the channels of mesopores in the silica shell can be easily opened by the deswelled polymer and drug molecules can pass through the mesopores more easily. It is expected that DOX is sufficiently stable in this nanocarrier with minimal drug leakage to reduce the toxic effects on normal tissues during circulation in the blood. Then, upon reaching the targeted tumor tissues, by the endocytosis of the enhanced permeability and retention (EPR) effect, the rapid release of DOX from the nanocarrier would be expected in the weakly acidic environment of tumor tissue and the further decreased pH value inside the endosome/lysosome compartments after cellular uptake, to introduce cell death. Such intelligent system would effectively decrease the side effects and toxicity of DOX and maximum the accumulation in tumor tissues. Meanwhile, we can monitor the cumulative release of DOX through the correlation between the UC emission intensity of the DOX-UCNPs@mSiO$_2$- P(NIPAm-*co*-MAA) hybrid nanospheres. It has been known that the DOX absorption peak covers the broad range from 400–580 nm, which overlaps with the green emission of UCNPs. Therefore, the UC emission intensity of the hybrid nanospheres has been quenched to a great extent after DOX loaded. As given in Figure 4D, the UC emission intensity increases with the release amount of DOX. The emission intensity reaches its maximum after drug release process is completely stopped. This correlation between the emission intensity and drug release extent can be potentially used as a probe to monitor the drug release process and efficiency in the course of the disease therapy.

Near-infrared (NIR) radiation are of current interest because they hold great promise as highly efficacious tools in the area of bio-applications. The laser of 980 nm is widely used as laser source to excite the photons of lanthanide based uponversion nanoparticles because the $^2F_{7/2} \rightarrow ^2F_{5/2}$ transition of Yb^{3+} has a larger absorption cross section than that of other lanthanide ions. Additionally, the $^2F_{7/2} \rightarrow 2F_{5/2}$ transition of Yb^{3+} is well resonant with many f–f transitions of typical upconverting lanthanide ions (Er^{3+}, Tm^{3+}, and Ho^{3+}). Water is the major absorbers of visible and infrared light and the absorption coefficient of water in the NIR region around 980 nm is not the lowest.[8,c,,27] As a result, continuous NIR radiation can effectively cause excessive local heating which can also be a powerful instrument to control drug release. Thus, a promotional effect of NIR irradiation on the DOX release was observed experimentally. DOX-UCNPs@mSiO$_2$-P(NIPAm-*co*-MAA) nanocomposites were incubated in PBS (pH = 7.4) for 1 h and then irradiated

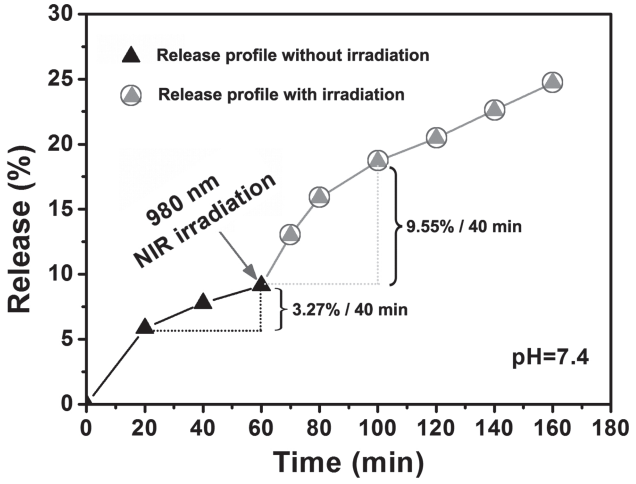

Figure 5. Release profiles of DOX from UCNPs@mSiO$_2$-P(NIPAm-*co*-MAA) nanocarriers in PBS buffer with or without laser irradiation at 980 nm at power density of 1.22 W.

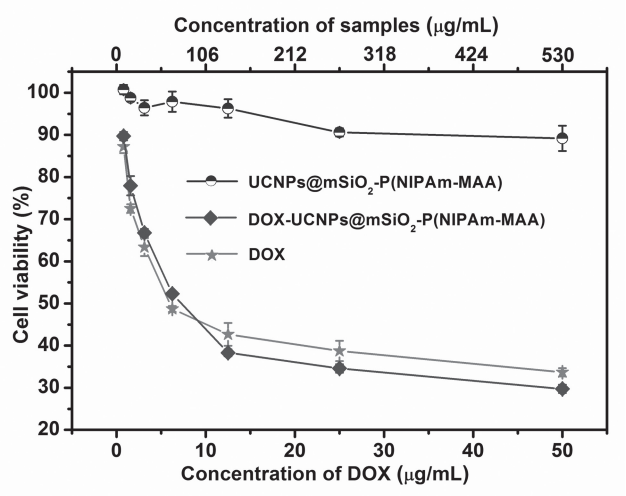

Figure 6. In vitro human HeLa ovarian cancer cell viabilities after 48 h incubation with free DOX, DOX-loaded UCNPs@mSiO$_2$-P(NIPAm-*co*-MAA) and bare UCNPs@mSiO$_2$-P(NIPAm-*co*-MAA) nanospheres at different concentrations.

with 1.22 W, 980 nm NIR laser. As can be seen from **Figure 5**, a burst release of DOX up to 9.55% was observed within 40 min. In comparison, only 3.27% DOX was released without irradiation. These results showed that NIR light enhanced drug release. The increased temperature induced by NIR irradiation cause the shrink of the polymer brushes and then the porous channels was forced to open and simultaneously leak out the drug molecules.

2.4. In Vitro Cytotoxic Effect and Cellular Uptake

To compare the pharmacological efficacy of the DOX-hybrid nanospheres and free DOX, HeLa cells were incubated in culture medium in the presence of free DOX, DOX-UCNPs@mSiO$_2$-P(NIPAm-*co*-MAA) and UCNPs@mSiO$_2$-P(NIPAm-*co*-MAA) with various concentrations for 24 h, and then MTT assay was used in vitro for quantitative testing of the cell viability. As presented in **Figure 6**, The blank UCNPs@mSiO$_2$-P(NIPAm-*co*-MAA) without DOX had low cytotoxic effect on cell viability even after 48 h treatment with the samples at the concentration as high as 530 μg/mL, showing satisfactory results that supported the biocompatibility of the carrier in all dosages. In contrast, both free DOX and DOX-loaded UCNPs@mSiO$_2$-P(NIPAm-*co*-MAA) exhibited suppression effect on cancer cell, which shows an increasing inhibition against Hela cell with increasing concentrations. About 70.3% of cells were killed by the DOX-UCNPs@mSiO$_2$-P(NIPAm-*co*-MAA) particles at an equivalent DOX concentration of 50 μg/mL. Meanwhile, free DOX exhibited slightly higher cytotoxicity than DOX-loaded nanospsheres at lower concertration and the result inversed when the concentration of DOX is up to 12.5 μg/mL. This result suggests that the cytotoxicity of DOX-UCNPs@mSiO$_2$-P(NIPAm-*co*-MAA) origins from the released DOX molecules after endocytic uptake by cancer cells. This can be explained to the reason that small molecules like DOX can be diffused into cells rapidly whereas the nanospheres have to be endocytosed to enter the cells.[28] Therefore, free DOX is faster than the DOX-loaded nanospheres by cellular uptake, which results in higher cytotoxicity at lower concentration. The higher cytotoxicity of DOX-UCNPs@mSiO$_2$-P(NIPAm-*co*-MAA) nanoparticles than free DOX molecules at higher concentration can be explained by the high uptake of DOX-UCNPs@mSiO$_2$-P(NIPAm-*co*-MAA) particles by HeLa cells through endocytosis, followed by the low-pH induced release of the loaded DOX inside the endosomal compartment.

Cellular-uptake characteristics of DOX-loaded UCNPs@mSiO$_2$-P(NIPAm-*co*-MAA) nanospheres were investigated by using flow cytometry and confocal laser scanning microscope (CLSM). Since DOX is a fluorophore, the fluorescence intensity could be also used to evaluate the intracellular activity of the obtained nanocomposites into a cancer cell line. The UCNPs@mSiO$_2$-P(NIPAm-*co*-MAA) nanoparticles were used to deliver DOX to the cells. The cell uptake degree of the nanocomposites could be quantified with flow cytometry by determining the signal of DOX loaded UCNPs@mSiO$_2$-P(NIPAm-*co*-MAA) nanospheres treated with HeLa cells. As shown in **Figure 7**A, after incubation of HeLa cells with the samples for different time intervals (30 min, 3 h, and 6 h), the median fluorescence levels in the PE-A histograms indicate that DOX-UCNPs@mSiO$_2$-P(NIPAm-*co*-MAA) nanocomposites were taken up by HeLa cells compared to the controlled cells, and the cell uptake amount increases gradually with the extension of the incubation time. In addition to the flow cytometry measurements, CLSM provide visible evidences that further verify the location of the UCNPs@mSiO$_2$-P(NIPAm-*co*-MAA) relative to the HeLa cells. The CLSM photographs of HeLa cells incubated with DOX loaded UCNPs@mSiO$_2$-P(NIPAm-*co*-MAA) for 1 h were shown in Figure 7B, where intracellular red fluorescence was observed, localized in the perinuclear area of the cytoplasm, demonstrating that the DOX loaded hybrid nanocarrier have been taken up by HeLa cells. The above results confirm that the

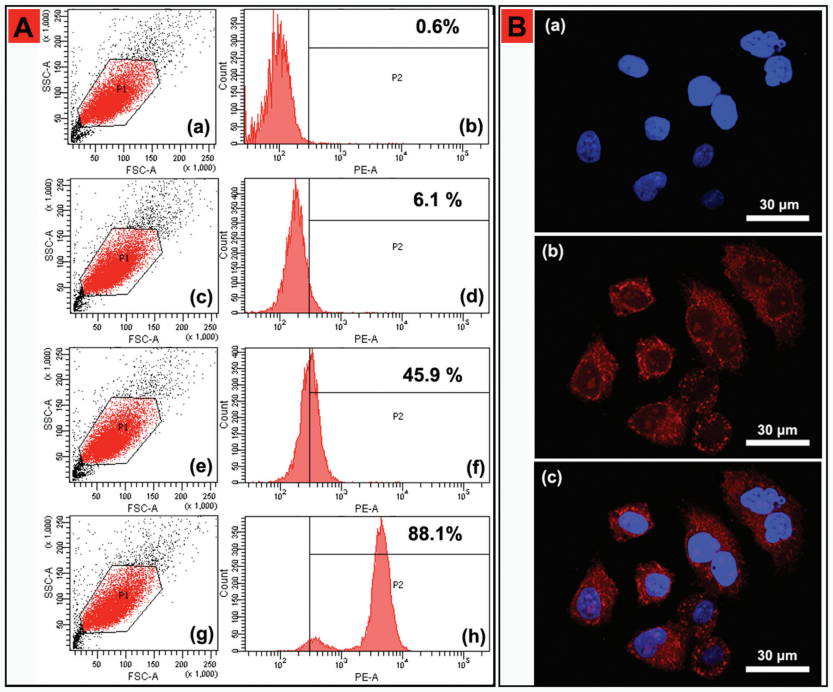

Figure 7. A) Flow cytometry analysis of the control cells (a,b) and HeLa cells incubated with DOX-loaded UCNPs@$mSiO_2$-P(NIPAm-co-MAA) nanocomposite spheres for 30 min (c,d), 3 h (e,f) and 6 h (g,h). B) CLSM image of HeLa cells incubated with DOX-UCNPs@$mSiO_2$-P(NIPAm-*co*-MAA) for 1 h at 37 °C. Each series can be classified to the nuclei of cells (being dyed in blue by Hoechst 100 33342 for visualization), DOX-loaded UCNPs@$mSiO_2$-P(NIPAm-*co*-MAA) composite and the merge of the two channels of both above, respectively.

UCNPs@$mSiO_2$-P(NIPAm-*co*-MAA) nanocarrier can be effectively taken up by HeLa cells. Thus, the effective therapy may result from the enhanced intracellular delivery, the temperature/pH-sensitive release and the protection of DOX extracellular by DOX-UCNPs@$mSiO_2$-P(NIPAM-*co*-MAA) nanocomposites.

2.5. Biomedical Imaging of UCNPs@ $mSiO_2$-P(NIPAm-*co*-MAA)

Lanthanide-doped up-conversion materials have been proven to be a promising tool for biomedical imaging and cancer therapy. In our present work, we also used time course up-conversion luminescence microscopy (UCLM) to investigate the interaction between human alveolar adenocarcinoma cells and the UCNPs@$mSiO_2$-P(NIPAm-*co*-MAA) hybrid nanospheres by utilizing a modified inverted fluorescence microscopy equipped with infrared laser excitation at 980 nm. After UCNPs@$mSiO_2$-P(NIPAm-*co*-MAA) (200 μg mL^{-1}) were incubated with A549 cells at 37 °C for 30 min, 1 h, and 6 h at 37 °C, abundant PBS was used to remove surface-attached nanospheres. The cells were investigated by UCLM with an external 980 nm laser as the excitation source. We can see that the obvious UCL signal coming from UCNPs@$mSiO_2$-P(NIPAm-*co*-MAA) nanoparticles inside A549 cells (**Figure 8**). The bright green luminescence signal can be observed in the dark, agreeing well with the corresponding UC luminescent spectrum. Overlays of bright field and UC luminescent images further demonstrate that the luminescence was evident in the intracellular region. Meanwhile, more and more UCNPs@$mSiO_2$-P(NIPAm-*co*-MAA) hybrid nanospheres were internalized into the cells as the time was prolonged from 10 min to 6 h. This indicates that UCNPs@$mSiO_2$-P(NIPAm-*co*-MAA) hybrid nanospheres penetrate the cell membrane of cells, agreeing well with the CLSM results. These observations confirm the capability of UCNPs@$mSiO_2$-P(NIPAm-*co*-MAA) for high-contrast in vitro cell imaging with negligible background. All the results demonstrate that UCNPs@$mSiO_2$-P(NIPAm-*co*-MAA) nanocarrier can also be used as an excellent luminescence probe for cell imaging and monitoring the cell endocytosis process.

3. Conclusion

In summary, we have designed a multifunctional nanoplatform for "detect and treat" strategy, by a combination of smart stimuli-responsive drug release and fluorescence imaging, for a promising possibility of cancer theranostics. The multimodal hybrid nanocarriers were

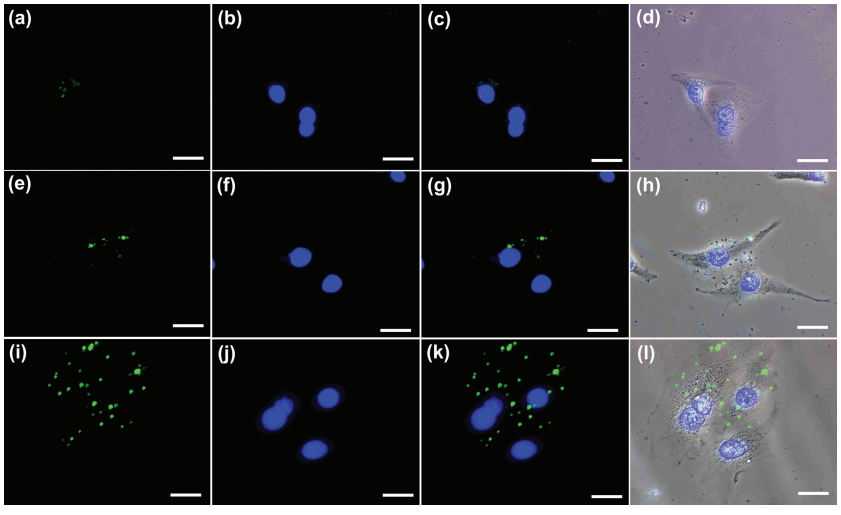

Figure 8. Inverted florescence microscope images of A549 cell line incubated with UCNPs@$mSiO_2$-P(NIPAm-*co*-MAA) nanospheres for 30 min (a–d), 1 h (e–h) and 6 h (i–l) at 37 °C. Each series can be classified to the upconversion luminescent image (UCL), nuclei of cells (being dyed in blue by Hoechst 33342 for visualization), and the overlay at dark-field image and bright-field image, respectively. Scare bars for all images are 25 μm.

composed of a UCNP core, a mesoporous silica shell, and pH and temperature-responsive P(NIPAm-*co*-MAA) polymer brush gatekeepers, forming an excellent platform for therapy and cell imaging. The as-prepared UCNPs@mSiO_2-P(NIPAm-*co*-MAA) nanocomposite shows the attracting properties of good biocompatibility, excellent stability and UC emission, which are suitable for anti-cancer drug (DOX) storage/release as a drug carrier. The drug-loaded particles are allowed the triggered release of the encapsulated DOX at higher temperature/low pH which depended on the swelling or deswelling of polymer locating the interstitial and surface layer and the behavior is consist with the tumor extracellular environment. Moreover, the NIR-light can promote the drug release by the heating effect- induced polymer collapse. Cell viability assays showed that DOX-loaded UCNPs@mSiO_2-P(NIPAm-*co*-MAA) nanospheres exhibited the similar cytotoxicity compared with free DOX at the same concentration. Moreover, UCLM images of UCNPs@mSiO_2-P(NIPAm-*co*-MAA) uptake by cells shows bright NIR UC emission, making the UCNPs@mSiO_2-P(NIPAm-*co*-MAA) promising candidates for use as bioimaging agents. With combining bioimaging and NIR-induced drug release for chemotheraphy in cancer theraphy simultaneously, this proof of concept might open the door to a new generation of carrier materials. Therefore, these unique properties of the hybrid nanocarriers could provide an opportunity for aid of a new generation of drug carrier which possesses a decision making process for smart site, time and dose-selected drug release and cell imaging.

4. Experimental Section

Chemicals and Materials: The rare earth oxides Y_2O_3, Yb_2O_3 and Er_2O_3 (99.999%) were purchased from Science and Technology Parent Company of Changchun Institute of Applied Chemistry. Sodium oleate ($C_{15}H_{33}NaO_2$, chemically pure, C. P.) and n-hexane (C_6H_{14}, analytical reagent, A.R.) were obtained from Sinopharm Chemical Reagent Co., Ltd. Oleic acid (OA), 1-octadecene (ODE) were purchased from Aldrich. Trichloromethane ($CHCl_3$, A.R.), sodium fluoride (NaF, guaranteed reagent, G.R.), 1,6-dioxane and ethanol (C_2H_5OH, A.R.) were purchased from Beijing Fine Chemical Company. Cetyltrimethylammonium bromide (CTAB, ≥ 99%), Tetraethyl orthosilicate (TEOS, A.R.), Ammonium nitrate (NH_4NO_3, ≥99.0%) and NaOH (reagent grade, ≥98%) were purchased from Beijing Yili Fine Chemical Regent Company (China).*N*-Isopropylacrylamide (NIPAm) was obtained from Sigma-Aldrich and recrystallized from a toluene-hexane solvent. Methacrylic acid (MAA) and methacryloxypropyltrimethoxysilane (MPS) were obtained from Aladdin. Diphenyl(2, 4, 6-trimethylbenzoyl)-phosphine oxide (TPO) was purchased from Tokyo Kasei Kogyo Co., Ltd. Doxorubicin hydrochloride (DOX) was purchased from Nanjing Duodian Chemical Limited Company (China).

Synthesis of $NaYF_4$:Yb/Er (18/2 mol%) Upconversion Nanoparticles (UCNPs): A literature method for the synthesis of iron-oleate complex was adopted to prepare the rare earth (RE) oleate complexes RE(oleate)$_3$.[29] Then the uniform UCNPs were synthesized by thermal decomposition methodology in high boiling point solvents and stabilized with oleic acid.[30] Typically, 1 mmol of RE(oleate)$_3$ (RE = 80%Y+ 18%Yb + 2%Er), 12 mmol of NaF, 10 mL of OA and 10 mL of ODE were added into a 100 mL three-neck round-bottom reaction vessel. The resulting mixture was slowly heated to 110 °C under a vacuum with magnetic stirring for 30 min to remove residual water and oxygen, and flushed periodically with N_2. Subsequently, the reaction was stabilized at 320 °C for 90 min in N_2 atmosphere under vigorous stirring to obtain the hydrophobic nanocrystals. When the reaction was completed, the transparent yellowish reaction mixture was allowed to cool to 70 °C before the excess ethanol was added. The obtained NCs were isolated by centrifugation and washed by ethanol and cyclohexane alternately. The as-prepared NCs could be readily dispersed in nonpolar solvents such as cyclohexane, toluene, and chloroform to form a colorless transparent colloid solution. The UCNPs were stabilized with oleic acid and dispersed in chloroform with a concentration of 6.5 mg L^{-1}.

Synthesis of UCNPs @mSiO_2 Composite Nanospheres: Mesopores silica directly coated-UCNPs were prepared similarly as described previously for the synthesis of silica coated hydrophobic Fe_3O_4 nanoparticles by Hyeon's group.[2d] Briefly, uniform OA coated UCNPs were transferred to an aqueous phase using cationic surfactant CTAB. A typical formation process of mesoporous silica coating was performed by self-assembly of the CTAB and silica precursor TEOS in basic solution. In a typical procedure, 0.5 mL of the prepared UCNPs in chloroform was poured into 5 mL of aqueous CTAB solution (0.055 M), and the resulting trubid oil-in-water microemulsion was stirred and sonicated vigorously for 30 min. Then, the mixture was heated up to 70 °C and aged for 10 min under stirring to evaporate the chloroform, resulting in a transparent solution. When the temperature was stable, the resulting solution was added to a mixture of water (45 mL), NaOH solution (0.3 mL, 2 M), certain amount of tetraethylorthosilicate (TEOS) and ethylacetate (3 mL) in sequence and the solution was stirred for 3 h. It is noteworthy that TEOS should be added dropwise and the mixture must be stirred heavily. After the reaction was completed, the as-synthesized UCNPs@mSiO_2 composite nanospheres were washed 3 times with ethanol to remove the unreacted species and dispersed in 10 mL of ethanol. To extract CTAB from the NPs, ion exchange method was used.[31] Typically, 100 mg of as-synthesized UCNPs@mSiO_2 powder was dispersed 25 mL of ethanol solution containing 0.25 g of NH_4NO_3 and refluxed at 80 °C for 6 h. The above treatment was repeated twice. The solid product was washed with water and ethanol several times and then dried at 60 °C for 12 h.

Synthesis of UCNPs@mSiO_2-P(NIPAm-co-MAA) Organic-Inorganic Hybrid Materials: To functionalize the surface of UCNPs@mSiO_2 nanospheres, the obtained particles were first modified by excessive amount of 3-(trimethoxysilyl)propylmethacrylate (MPS) to introduce double bond onto the pores and surface of mesoporous silica shell. The desired amount of UCNPs@mSiO_2 composite nanospheres were redispersed in 30 mL of pure ethanol and 200 μL of MPS was added dropwise to the dispersion under continuous stirring with a magnetic stirrer. After stirred for 24 h at 30 °C, the dispersion was refluxed for 1 h to ensure covalent binding. Afterwards, the dispersions were cooled to room temperature, washed with ethanol for several times and then dried at 60 °C for 12 h.

UCNPs@SiO_2-P(NIPAm-*co*-MAA) composites were achieved by a facial photo-induced polymerization. NIPAm (0.125 g), MAA (7.6 uL), and TPO (0.003 g, photoinitiator) were dissolved in 500 uL 1, 6-dioxane to form transparent solution and then 20 mg of UCNPs@mSiO_2-MPS powders were added. The suspension was sonicated for 30 min and further stirred overnight at room temperature in the dark. After that, the resulting monomer-contained nanoparticles were exposed to UV light (200 W cm^{-2}, LAMP, PHILIPS) for 8 min to make the photo-initiated polymerization take place. After that, the prepared product was washed with ethanol and water for several times to remove unreacted monomers and impurities, then dried in vacuum at 50 °C to obtain the final samples, denoted as UCNPs @mSiO2-P(NIPAm-*co*-MAA).

The Biocompatibility of the UCNPs@mSiO_2-P(NIPAm-co-MAA) Organic-Inorganic Composite Materials: To evaluate the biocompatibility of the UCNPs@mSiO_2-P(NIPAm-*co*-MAA) organic-inorganic hybrid materials, MTT cell assay was performed on the L929 fibroblast cells. MTT assay is a standard test for screening the toxicity of biomaterials and is carried out in accordance with ASTM standards. Briefly, L929 cells were plated out at a density of 5000–6000 cells per well in a 96 well plate, then incubated overnight at 37 °C in a humidified atmosphere of 5% CO_2 to allow the cells to attach to the wells. The UCNPs@mSiO_2-P(NIPAm-

co-MAA) composites were sterilized by autoclaving, and then serial dilutions of the nanocomposites at concentrations of 3.125, 6.25, 12.5, 25, 50, 100, and 200 μg mL^{-1} were added to the culture wells to replace the original culture medium and incubated for another 24 h in 5% CO_2 at 37 °C. 5 mg mL^{-1} stock solution of MTT [3–(4,5–dimethylthiazol–2–yl)–2,5–diphenyltetrazolium bromide] was prepared in PBS and this stock solution (20 μL) was added to each well containing a different amount of the monodisperse UCNPs@mSiO_2-P(NIPAm-*co*-MAA) for another 4 h. Then 150 μL of dimethyl sulfoxide (DMSO) was added to each well before the plate was examined using a microplate reader (Therom Multiskan MK3) at the wavelength of 490 nm.

Loading, Capping and Release Experiments: For doxorubicin loading, UCNPs@mSiO_2-P(NIPAm-*co*-MAA) samples were mixed with 2 mL of DOX aqueous solution (1 mg mL^{-1}). After being shaken for 24 h at 45 °C to reach the equilibrium state under dark conditions, the DOX-loaded samples were collected by centrifugation and the supernatant was collected for UV measurement to determine the adsorbed amount of DOX. Then, DOX loaded UCNPs@mSiO_2-P(NIPAm-*co*-MAA) samples were immersed in 2 mL pH = 7.4, 5.0 and 2.0 PBS buffer solutions at 45 °C and 25 °C respectively with gentle shaking. At predetermined time intervals, PBS was taken out and replaced with an equal volume of fresh PBS. The amount of released DOX in the supernatant solutions was measured by UV-vis spectrophotometer at a wavelength of 480 nm. The loading and release process of DOX loaded UCNPs@mSiO_2 samples were preceded following the same procedure.

In Vitro Cytotoxicity of DOX-Loaded UCNPs@mSiO_2-P(NIPAm-co-MAA) Nanospheres and Cell Viability: HeLa cells were plated out in 96-well plates at a density of 8000 cells per well and were allowed to attach and grow for 24 h to allow the cells to attach. The free DOX, DOX-loaded UCNPs@mSiO2-P(NIPAm-*co*-MAA), and UCNPs@mSiO_2-P(NIPAm-*co*-MAA) were added to the medium, and the cells were incubated in 5% CO2 at 37 °C for 24 h. The concentrations of DOX were 1.5625, 3.125, 6.25, 12.5, 25, 50 μg mL^{-1} respectively and the correlative concentrations of UCNPs@mSiO_2- P(NIPAm-*co*-MAA) were 8.25, 16.5, 33.2, 66.3, 133, 265, 530 μg mL^{-1}, respectively. Before removing the media in the composites, 20 μL of MTT solution was added into each cell and incubated for another 4 h. Cell viability was also determined using MTT assay, which was the same as the procedure mentioned above.

Cellular Uptake of the UCNPs@mSiO_2-P(NIPAm-co-MAA): Cellular uptake by HeLa cells was examined using confocal laser scanning microscope (CLSM) and flow cytometry respectively. For CLSM, the Hela cells were seeded in 6-well culture plates (a clean cover slip was put in each well) and grown overnight as a monolayer, and were incubated with free DOX, DOX-loaded UCNPs@mSiO_2-P(NIPAm-*co*-MAA) nanocomposites and UCNPs@mSiO_2-P(NIPAm-*co*-MAA) nanospheres at 37 °C for 1 h. Thereafter, the cells were rinsed with PBS three times, fixed with 2.5% formaldehyde (1 mL/well) at 37 °C for 10 min, and then rinsed with PBS three times again. For nucleus labeling, the nuclei was stained with Hoechst 33342 solution (from Molecular Probes, 20 mg mL^{-1} in PBS, 1 mL/well) for 10 min and then rinsed with PBS three times. The cover slips were placed on a glass microscope slide, and the samples were visualized using CLSM (FV10-ASW).

For flow cytometry studies, HeLa cells (1×10^6) were seeded in 6-well culture plates and grown overnight. The cells were then treated with DOX-loaded UCNPs@mSiO_2-P(NIPAm-*co*-MAA) at 37 °C for 30 min, 3 h and 6 h. A single cell suspension was prepared consecutively by trypsinization, washing with PBS, and filtration through 35 mm nylon mesh. Thereafter, the cells were lifted using a cell stripper (Media Tech. Inc.), and analyzed using a FACSCalibur flow cytometer (BD Biosciences) for DOX. The excitation wavelength and emission wavelength were 488 nm and 575 nm, respectively.

Upconversion Luminescence Imaging of UCNPs@mSiO_2-P(NIPAm-co-MAA): The instrument of up-conversion luminescence microscopy (UCLM) was rebuilt on an inverted florescence microscope (Nikon Ti-S), an infrared laser excited unit (FF735-Di01-25 × 36, Nikon) and laser diode driver (KS3-11312-312, BWT). UC luminescence (UCL) bioimaging of A549 cell (5×10^4/well) were seeded in 6-well culture plates (a clean cover slip was put in each well) and grown overnight as a monolayer, and were incubated with DOX-UCNPs@mSiO_2-P(NIPAm-*co*-MAA) at 37 °C for 4 h. Thereafter, the cells were washed with PBS three times, fixed with 2.5% formaldehyde at 37 °C for 10 min, and then washed with PBS three times again. UCLM imaging was performed with the reconstructive Nikon Ti-S. Cells were excited by infrared laser at 980 nm (BWT Beijing LTD, China) with output power of 250 mW.

Characterization: XRD was performed on a D8 Focus diffractometer (Bruker) with Cu Ka radiation (0.15405 nm). Transmission electron microscopy (TEM) images were recorded on a FEI Tecnai G2 S-Twin transmission electron microscope with a field emission gun operating at 200 kV. Fourier-transform Infrared (FT-IR) spectra were measured on a Vertex Perkin–Elmer 580BIR spectrophotometer (Bruker) with the KBr pellet technique. N_2 adsorption/desorption isotherms were obtained on a Micromeritics ASAP 2020 M apparatus. Pore size distribution was calculated from the adsorption branch of N_2 adsorption/desorption isotherm and the Barret–Joner–Halenda (BJH) method. Zeta-potential measurements were carried out on Malvern Zetasizer Nano ZS system (Malvern Instruments Ltd., England). The BET surface areas were determined using the data between 0.05 and 0.35 just before the capillary condensation, and the pore volume was obtained by the t-plot method. Thermogravimetry (TG) was carried out on a Netzsch Thermoanalyzer STA 409 instrument in an atmospheric environment with a heating rate of 10 °C/min from room temperature to 800 °C. The UV-vis absorption spectra values were measured on a U-3310 spectrophotometer. The UC emission spectra were taken on an F-7000 spectrophotometer (Hitachi) equipped with a 980 nm laser (BWT Beijing LTD., China) as the excitation source. Gel permeation chromatography (GPC) measurements were conducted with a Waters 410 GPC with $CHCl_3$ as eluent (flow rate of 1 mL min^{-1}, at 35 °C) and the molecular weights were calibrated with polystyrene standards. Flow cytometry analysis was performed on FACSCalibur flow cytometer (BD Biosciences) with 488 nm excitation lasers. CLSM images were observed by confocal laser scanning microscope (Olympus, FV 1000).

Supporting Information

Supporting Information is available from the Wiley Online Library or from the author.

Acknowledgements

This project was financially supported by the National Basic Research Program of China (2010CB327704), National High Technology Program of China (2011AA03A407), the National Natural Science Foundation of China (NSFC 51172228, 51272248, 20901074, 21221061) and Science Technology Development Program of Jilin Province for Youths (20100106).

Received: January 13, 2013
Revised: February 7, 2013
Published online: March 27, 2013

[1] a) N. M. Idris, M. K. Gnanasammandhan, J. Zhang, P. C. Ho, R. Mahendran, Y. Zhang, *Nat. Med.* **2012**, *18*, 1580; b) J. Kim, S. Park, J. E. Lee, S. M. Jin, J. H. Lee, I. S. Lee, I. Yang, J.-S. Kim, S. K. Kim, M.-H. Cho, T. Hyeon, *Angew. Chem. Int. Ed.* **2006**, *45*, 7754; c) F. Zhang, G. B. Braun, A. Pallaoro, Y. Zhang, Y. Shi, D. Cui, M. Moskovits, D. Zhao, G. D. Stucky, *Nano Lett.* **2012**, *12*, 61.

[2] a) P. Zrazhevskiy, M. Sena, X. Gao, *Chem. Soc. Rev.***2010** *39*, 4326; b) J. Kim, Y. Piao, T. Hyeon, *Chem. Soc. Rev.* **2009**, *38*, 372; c) M. Ma, H. Chen, Y. Chen, X. Wang, F. Chen, X. Cui, J. Shi, *Biomaterials* **2012**, *33*, 989; d) J. Kim, H. S. Kim, N. Lee, T. Kim, H. Kim,

T. Yu, I. C. Song, W. K. Moon, T. Hyeon, *Angew. Chem. Int. Ed.* **2008**, *47*, 8438; e) Q. Liu, M. Chen, Y. Sun, G. Chen, T. Yang, Y. Gao, X. Zhang, F. Li, *Biomaterials* **2011**, *32*, 8243.

[3] a) W. C. W. Chan, S. Nie, *Science* **1998**, *281*, 2016; b) J.-H. Park, L. Gu, G. von Maltzahn, E. Ruoslahti, S. N. Bhatia, M. J. Sailor, *Nat. Mater.* **2009**, *8*, 331; c) H. Kobayashi, M. Ogawa, R. Alford, P. L. Choyke, Y. Urano, *Chem. Rev.* **2009**, *110*, 2620; d) J. M. Klostranec, W. C. W. Chan, *Adv. Mater.* **2006**, *18*, 1953; e) J. Zhou, Y. Sun, X. Du, L. Xiong, H. Hu, F. Li, *Biomaterials* **2010**, *31*, 3287; f) M. Nyk, R. Kumar, T. Y. Ohulchanskyy, E. J. Bergey, P. N. Prasad, *Nano Lett.* **2008**, *8*, 3834; g) L. Cao, X. Wang, M. J. Meziani, F. Lu, H. Wang, P. G. Luo, Y. Lin, B. A. Harruff, L. M. Veca, D. Murray, S.-Y. Xie, Y.-P. Sun, *J. Am. Chem. Soc.* **2007**, *129*, 11318; h) X. He, J. Gao, S. S. Gambhir, Z. Cheng, *Trends Mol. Med.* **2010**, *16*, 574; i) Y. Yang, Q. Shao, R. Deng, C. Wang, X. Teng, K. Cheng, Z. Cheng, L. Huang, Z. Liu, X. Liu, B. Xing, *Angew. Chem. Int. Ed.* **2012**, *51*, 3125.

[4] a) S. Wu, G. Han, D. J. Milliron, S. Aloni, V. Altoe, D. V. Talapin, B. E. Cohen, P. J. Schuck, *Proc. Natl. Acad. Sci. USA* **2009**, *106*, 10917; b) Y. I. Park, J. H. Kim, K. T. Lee, K.-S. Jeon, H. Bin Na, J. H. Yu, H. M. Kim, N. Lee, S. H. Choi, S.-I. Baik, H. Kim, S. P. Park, B.-J. Park, Y. W. Kim, S. H. Lee, S.-Y. Yoon, I. C. Song, W. K. Moon, Y. D. Suh, T. Hyeon, *Adv. Mater.* **2009**, *21*, 4467.

[5] Z. Li, Y. Zhang, S. Jiang, *Adv. Mater.* **2008**, *20*, 4765.

[6] Q. Liu, Y. Sun, T. Yang, W. Feng, C. Li, F. Li, *J. Am. Chem. Soc.* **2011**, *133*, 17122.

[7] C. Wang, H. Tao, L. Cheng, Z. Liu, *Biomaterials* **2011**, *32*, 6145.

[8] a) F. Wang, X. Liu, *Chem. Soc. Rev.* **2009**, *38*, 976; b) J. Zhou, Z. Liu, F. Y. Li, *Chem. Soc. Rev.* **2012**, *41*, 1323; c) R. Weissleder, *Nat. Biotechnol.* **2001**, *19*, 316; d) D. Tu, L. Liu, Q. Ju, Y. Liu, H. Zhu, R. Li, X. Chen, *Angew. Chem. Int. Ed.* **2011**, *50*, 6306; e) D. Tu, L. Liu, Q. Ju, Y. Liu, H. Zhu, R. Li, X. Chen, *Angew. Chem. Int. Ed.* **2011**, *50*, 6306; f) T. Tu, S. Li, M. Zhu, F. Li, L. Q. Liu, X. Chen, *Nanoscale* **2013**, *5*, 1369; g) W. Luo, C. Fu, R. Li, Y. Liu, H. Zhu, X. Chen, *Small* **2011**, *7*, 3046; h) Y. Liu, D. Tu, H. Zhu, R. Li, W. Luo, X. Chen, *Adv. Mater.* **2010**, *22*, 3266; i) Q. Ju, D. Tu, Y. Liu, R. Li, H. Zhu, J. Chen, Z. Chen, M. Huang, X. Chen, *J. Am. Chem. Soc.* **2012**, *134*, 1323.

[9] a) Q. Liu, T. Yang, W. Feng, F. Li, *J. Am. Chem. Soc.* **2012**, *134*, 5390; b) L. Cheng, K. Yang, Y. Li, J. Chen, C. Wang, M. Shao, S.-T. Lee, Z. Liu, *Angew. Chem. Int. Ed.* **2011**, *50*, 7385; c) J. Zhou, Z. Yang, W. Dong, R. Tang, L. Sun, C. Yan, *Biomaterials* **2011**, *32*, 9059; d) H. Xu, L. Cheng, C. Wang, X. Ma, Y. Li, Z. Liu, *Biomaterials* **2011**, *32*, 9364; e) M. Wang, C. Mi, W. Wang, C. Liu, Y. Wu, Z. Xu, C. Mao, S. Xu, *ACS Nano* **2009**, *3*, 1580; f) H. Xing, W. Bu, S. Zhang, X. Zheng, M. Li, F. Chen, Q. He, L. Zhou, W. Peng, Y. Hua, J. Shi, *Biomaterials* **2012**, *33*, 1079; g) R. Kumar, M. Nyk, T. Y. Ohulchanskyy, C. A. Flask, P. N. Prasad, *Adv. Funct. Mater.* **2009**, *19*, 853; h) M. K. G. Jayakumar, N. M. Idris, Y. Zhang, *Proc. Natl. Acad. Sci. USA* **2012**, *109*, 8483; i) D. Tu, Y. Liu, H. Zhu, R. Li, L. Liu, X. Chen, *Angew. Chem. Int. Ed.* **2013**, *52*, 1128; j) X. Zhang, P. Yang, C. Li, D. Wang, J. Xu, S. Gai, J. Lin, *Chem. Commun.* **2011**, *47*, 12143.

[10] a) J. Liu, W. Bu, S. Zhang, F. Chen, H. Xing, L. Pan, L. Zhou, W. Peng, J. Shi, *Chem. Eur. J.* **2012**, *18*, 2335; b) Z. Li, Y. Zhang, *Angew. Chem. Int. Ed.* **2006**, *45*, 7732; c) S. Gai, P. Yang, C. Li, W. Wang, Y. Dai, N. Niu, J. Lin, *Adv. Funct. Mater.* **2010**, *20*, 1166.

[11] a) I. I. Slowing, J. L. Vivero-Escoto, C.-W. Wu, V. S. Y. Lin, *Adv. Drug Delivery Rev.* **2008**, *60*, 1278; b) M. Vallet-Regi, F. Balas, D. Arcos, *Angew. Chem. Int. Ed.* **2007**, *46*, 7548; c) T. Lebold, C. Jung, J. Michaelis, C. Braeuchle, *Nano Lett.* **2009**, *9*, 2877; d) B. G. Trewyn, I. I. Slowing, S. Giri, H.-T. Chen, V. S. Y. Lin, *Acc. Chem. Res.* **2007**, *40*, 846; e) S. Saha, K. C. F. Leung, T. D. Nguyen, J. F. Stoddart, J. I. Zink, *Adv. Funct. Mater.* **2007**, *17*, 685; f) F. Hoffmann, M. Cornelius, J. Morell, M. Fröba, *Angew. Chem. Int. Ed.* **2006**, *45*, 3216.

[12] a) C. D. H. Alarcon, S. Pennadam, C. Alexander, *Chem. Soc. Rev.* **2005**, *34*, 276; b) E. S. Gil, S. M. Hudson, *Prog. Polym. Sci.* **2004**, *29*, 1173.

[13] a) F. Torney, B. G. Trewyn, V. S. Y. Lin, K. Wang, *Nat. Nanotechnol.* **2007**, *2*, 295. b) J. L. Vivero-Escoto, I. I. Slowing, C.-W. Wu, V. S. Y. Lin, *J. Am. Chem. Soc.* **2009**, *131*, 3462. c) F. Muharnmad, M. Guo, W. Qi, F. Sun, A. Wang, Y. Guo, G. Zhu, *J. Am. Chem. Soc.* **2011**, *133*, 8778.

[14] a) N. K. Mal, M. Fujiwara, Y. Tanaka, *Nature* **2003**, *421*, 350; b) S. Angelos, Y.-W. Yang, K. Patel, J. F. Stoddart, J. I. Zink, *Angew. Chem. Int. Ed.* **2008**, *47*, 2222; c) C. Park, H. Kim, S. Kim, C. Kim, *J. Am. Chem. Soc.* **2009**, *131*, 16614.

[15] a) R. Liu, X. Zhao, T. Wu, P. Feng, *J. Am. Chem. Soc.* **2008**, *130*, 14418; b) Y. Qiu, K. Park, *Adv. Drug Delivery Rev.* **2001**, *53*, 321; c) B. Jeong, S. W. Kim, Y. H. Bae, *Adv. Drug Delivery Rev.* **2012**, *64*, 154.

[16] a) L. A. Perelman, T. Moore, J. Singelyn, M. J. Sailor, E. Segal, *Adv. Funct. Mater.* **2010**, *20*, 826; b) J. Guo, W. Yang, C. Wang, J. He, J. Chen, *Chem. Mater.* **2006**, *18*, 5554; c) Y.-Z. You, K. K. Kalebaila, S. L. Brock, D. Oupicky, *Chem. Mater.* **2008**, *20*, 3354; d) C. Liu, J. Guo, W. Yang, J. Hu, C. Wang, S. Fu, *J. Mater. Chem.* **2009**, *19*, 4764. e) Y. Z. Pan, H. Q. Bao, N. G. Sahoo, T. F. Wu, L. Li, *Adv. Funct. Mater.* **2011**, *21*, 2754; f) A. Baeza, E. Guisasola, E. Ruiz-Hernandez, M. Vallet-Regi, *Chem. Mater.* **2012**, *24*, 517; g) Y. F. Yang, A. J. Mijalis, H. Fu, C. Agosto, K. J. Tan, J. D. Batteas, D. E. Bergbreiter, *J. Am. Chem. Soc.* **2012**, *134*, 7378.

[17] a) D. Schmaljohann, *Adv. Drug Delivery Rev.* **2006**, *58*, 1655; b) M. Stubbs, P. M. J. McSheehy, J. R. Griffiths, C. L. Bashford, *Mol. Med. Today* **2000**, *6*, 15.

[18] V. Torchilin, *Eur. J. Pharm. Biopharm.* **2009**, *71*, 431.

[19] a) X. Kang, Z. Cheng, D. Yang, P. a. Ma, M. Shang, C. Peng, Y. Dai, J. Lin, *Adv. Funct. Mater.* **2012**, *22*, 1470; b) G. R. Hendrickson, M. H. Smith, A. B. South, L. A. Lyon, *Adv. Funct. Mater.* **2010**, *20*, 1697; c) N. S. Satarkar, J. Z. Hilt, *J. Controlled Release* **2008**, *130*, 246.

[20] B. Chang, X. Sha, J. Guo, Y. Jiao, C. Wang, W. Yang, *J. Mater. Chem.* **2011**, *21*, 9239.

[21] Y. Dai, P. a. Ma, Z. Cheng, X. Kang, X. Zhang, Z. Hou, C. Li, D. Yang, X. Zhai, J. Lin, *ACS Nano* **2012**, *6*, 3327.

[22] a) Z. Hou, C. Li, P. a. Ma, Z. Cheng, X. Li, X. Zhang, Y. Dai, D. Yang, H. Lian, J. Lin, *Adv. Funct. Mater.* **2012**, *22*, 2713; b) J. Kim, J. E. Lee, J. Lee, J. H. Yu, B. C. Kim, K. An, Y. Hwang, C. H. Shin, J. G. Park, T. Hyeon, *J. Am. Chem. Soc.* **2006**, *128*, 688; c) T. Kim, E. Momin, J. Choi, K. Yuan, H. Zaidi, J. Kim, M. Park, N. Lee, M. T. McMahon, A. Quinones-Hinojosa, J. W. M. Bulte, T. Hyeon, A. A. Gilad, *J. Am. Chem. Soc.* **2011**, *133*, 2955.

[23] H. Chen, C. Deng, X. Zhang, *Angew. Chem. Int. Ed.* **2010**, *49*, 607.

[24] N. Lewinski, V. Colvin, R. Drezek, *Small* **2008**, *4*, 26.

[25] F. Auzel, *Chem. Rev.* **2003**, *104*, 139.

[26] M. Haase, H. Schafer, *Angew. Chem. Int. Ed.* **2011**, *50*, 5808.

[27] J. Frangioni, *Curr. Opin. Chem. Biol.* **2003**, *7*, 626.

[28] J. Chen, X. Qiu, J. Ouyang, J. Kong, W. Zhong, M. M. Q. Xing, *Biomacromolecules* **2011**, *12*, 3601.

[29] P. Jongnam, A. Kwangjin, H. Yosun, P. Je-Geun, N. Han-Jin, K. Jae-Young, P. Jae-Hoon, H. Nong-Moon, H. Taeghwan, *Nat. Mater.* **2004**, *3*, 891.

[30] Y. Wei, F. Lu, X. Zhang, D. Chen, *Chem. Mater.* **2006**, *18*, 5733.

[31] N. Lang, A. Tuel, *Chem. Mater.* **2004**, *16*, 1961.